Eur. Phys. J. D **39**, 373–378 (2006)
DOI: 10.1140/epjd/e2006-00116-1

THE EUROPEAN PHYSICAL JOURNAL D

Radiative lifetimes of the NaRb $C(3)^1\Sigma^+$ state: experiment and theory

I. Klincare[1], M. Tamanis[1], R. Ferber[1,a], A. Zaitsevskii[2], E.A. Pazyuk[2], and A.V. Stolyarov[2]

[1] Department of Physics and Institute of Atomic Physics and Spectroscopy, University of Latvia, Riga 1586, Latvia
[2] Department of Chemistry, Moscow State University, Moscow 119899, Russia

Received 13 February 2006
Published online 7 June 2006 –

Abstract. Radiative lifetimes for $2 \leq v' \leq 44$ rovibronic $C^1\Sigma^+$ state levels of NaRb and quenching collision cross-sections with Rb atoms have been directly measured in a thermal cell by detecting time resolved laser induced fluorescence after pulsed excitation. Many body multipartitioning theory was applied to calculate $C^1\Sigma^+ - X^1\Sigma^+$ and $C^1\Sigma^+ - A^1\Sigma^+$ transition dipole moments. The relevant ab initio matrix elements were converted to the $C^1\Sigma^+$ state radiative lifetimes. The strong spin-orbit $A^1\Sigma^+ \sim b^3\Pi$ coupling effect on the total $C \rightarrow A$ transition probabilities and lifetimes of the $C^1\Sigma^+$ state is discussed. The measured radiative lifetimes show a decrease from 61 to 34 ns as the v' values increase, the results being in good agreement with calculations. The averaged collisional quenching cross-section value $\sigma = (3 \pm 1) \times 10^{-14}$ cm^2 was determined for NaRb ($C^1\Sigma^+$) + Rb collisions from the Stern-Volmer plots.

PACS. 33.70.Ca Oscillator and band strengths, lifetimes, transition moments, and Franck-Condon factors – 33.50.Hv Radiationless transitions, quenching

1 Introduction

The NaRb molecule is among prospective objects for two species laser cooling and photoassociative studies [1,2]. Designing optimal schemes to create ultracold molecules in their absolute ground state requires reliable information about the ground and excited electronic states in a wide range of internuclear distances (R) [3,4]. Therefore, accurate potential energy curves (PEC), permanent and transition dipole moments, and radiative lifetimes of the electronically excited states of mixed alkali dimers are of current interest. During last few years great efforts have been made to characterize theoretically and experimentally the structure of the NaRb molecule. In reference [5] the ab initio PECs of the ground and a number of excited electronic states were calculated up to their atomic asymptotes, see Figure 1. In reference [6] the ab initio PECs of the first 11 lowest electronic states were calculated up to $R = 7$ Å by applying many-body multipartitioning perturbation theory (MPPT). Presently the ground and several low lying excited electronic states of the NaRb molecule are characterized quite well experimentally. A very accurate ground $X^1\Sigma^+$ state empirical potential was obtained in [7,8] by means of Fourier transform spectroscopy analysis of the $D^1\Pi$ – $X^1\Sigma^+$, $B^1\Pi$ – $X^1\Sigma^+$ and $C^1\Sigma^+$ – $X^1\Sigma^+$ transitions in laser induced fluorescence (LIF). The $B^1\Pi$ state was studied in [9,10] by sub-Doppler polarization spectroscopy. First high resolution spectroscopy data on the $A^1\Sigma^+ - b^3\Pi$ complex were obtained in [11]. Recently, a high resolution spectroscopy study of the $D^1\Pi$ state was completed [12]. The $C^1\Sigma^+$ state was described in [13] by combining Fourier transform spectroscopy analysis of C–X transitions in LIF and polarization labelling spectroscopy methods. An accurate empirical PEC for the $C^1\Sigma^+$ state converging to the Na($3p$)+Rb($5s$) dissociation limit, see Figure 1, was obtained in the region of vibrational levels from $v' = 0$ to 64 [13]. The experiment confirmed the existence of the shelf region for the $C^1\Sigma^+$ state, which started at $R \approx 7.5$ Å as predicted by theory [5]. The shelf reflects an avoided crossing of the adiabatic $C^1\Sigma^+$ and $E^1\Sigma^+$ states having strong ionic/covalent mixing character.

As to radiative properties of NaRb, in reference [6] the ab initio MPPT transition dipole moment functions $d(R)$ for A, $C^1\Sigma^+ - X^1\Sigma^+$; B, $D^1\Pi - X^1\Sigma^+$; $D^1\Pi - A^1\Sigma^+$ and $D^1\Pi - B^1\Pi$ electronic transitions, along with respective PECs, were calculated in the interval $R \in [3, 7]$ Å. The relevant matrix elements were converted to radiative lifetimes τ_{rad} of the $D^1\Pi$ and $B^1\Pi$ states, and the τ_{rad} dependencies on vibrational–rotational v', J' levels of these states were obtained. The progress in spectroscopic analysis of the NaRb molecule made it possible to perform

[a] e-mail: ferber@latnet.lv

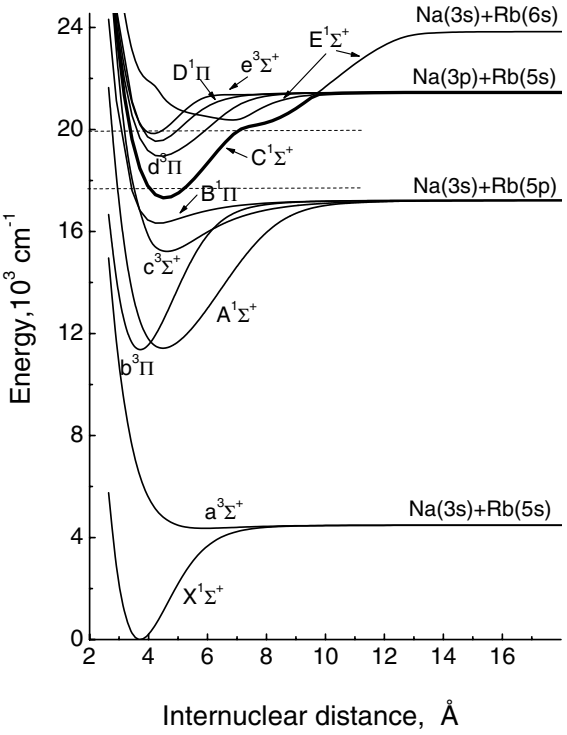

Fig. 1. Ab initio potential energy curves for the low-lying states of NaRb according to reference [5]. The area within the dotted horizontal lines shows the energy interval of the $C^1\Sigma^+$ state covered in present study.

a correct assignment of rovibronic levels under study and thus stimulated experimental vibrationally and rotationally selective lifetime studies of the excited electronic states. Collisionless radiative lifetime values for v', J' rovibronic levels in the $D^1\Pi$ state within v' range from 0 to 17 were directly measured in [14], with values monotonically decreasing from 22.5 to 17.3 ns with increasing v'. These results were in good agreement with calculated τ_{rad} dependencies [6] as well as with the very first lifetime value measured in [15]. It is worth noting that the lifetime value of 17.8 ns of the $B^1\Pi$ state level $v' = 5$, $J' = 20$ measured in [16] also agrees with its calculated value [6].

Recently Aymar and Dulieu have calculated ab initio transition moment $d(R)$ functions for several $^1\Sigma^+ - ^1\Sigma^+$ transitions in NaRb in a wide R-range by a core polarization pseudopotential (CPP) method, see discussion in [13], where their $d_{C-X}(R)$ function was exploited in order to analyze the applicability of the $C^1\Sigma^+$ – $X^1\Sigma^+$ transition for photoassociation studies.

The present paper is a continuation of our previous studies [6,14] of radiative properties of the NaRb molecule. We report in this work the first lifetime measurements for the NaRb $C^1\Sigma^+$ state in a wide v', J' range, although the highest measured level still lies just below the shelf region. The experiment is supported by radiative lifetime calculations based on ab initio $d(R)$ functions of the $C^1\Sigma^+$ – $X^1\Sigma^+$ and $C^1\Sigma^+$ – $A^1\Sigma^+$ transitions calculated in the present work with the MPPT method. Experimental effective total cross-sections of quenching collisions are reported as well.

2 Experiment

2.1 Experimental set-up

The experimental set-up has been described in [14], thus we will mention only some essential points. The NaRb molecules were produced in a thermal cell made from alkali-resistant glass by heating a mixture of rubidium (natural composition: 72% ^{85}Rb and 28% ^{87}Rb) and sodium metals in an approximate proportion 4:1 by weight. Before the experiments the cell was outgassed at ca. 400 °C, then filled under vacuum with the metals by distillation and sealed off. During the measurements the oven temperature was kept between 180–280 °C. To excite the C – X fluorescence we used the Ar^+ laser lines 514.5 nm, 501.7 nm (Spectra Physics 171, with intracavity etalon) and 528.7 nm (Spectra Physics BeamLok 2040, multimode regime), as well as a tunable single mode dye laser (Coherent CR 699-21) with Rhodamin 6G dye. The fluorescence was detected at right angles to the incident laser beam and dispersed by a DFS-12 double monochromator with a reciprocal dispersion of 0.5 nm/mm, which provided a spectral resolution of about 0.02 nm at reasonable slit widths.

The kinetic measurements were performed on the particular fluorescence lines of the C – X progression, which were singled out by the monochromator, and which originated from a selected excited v', J' level. The laser beam was modulated by a ML-102 electro-optical modulator at repetition rate of 850 kHz. The laser pulse parameters were: pulse width about 100 ns, rear front about 20 ns, and modulation depth better than 1:50. For the kinetic measurements the monochromator slits were kept at a width of 0.5–1 mm in order to provide a measurable fluorescence signal. The scattered laser light was cut off with colored glass filters placed before the entrance slit. At these conditions the LIF response detected with a photomultiplier (PMT) in photon counting regime did not exceed 3000 counts/s. One-photon pulses from the PMT were discriminated, amplified and formed to standard pulses (1 V, 10 ns duration) by fast electronics. The LIF decay was registered with a time-correlated single-photon counting technique with a time-to-amplitude convertor (TAC) and a multichannel amplitude analyzer (MCA). The time resolution of the system was estimated as 1.35 ns/channel with about 1% accuracy. The TAC was operated in inverse start-stop regime: the one-photon pulses from the PMT were used to start the TAC, whereas the stop-pulses came at a frequency of 850 kHz from the nanosecond generator synchronized with the laser modulation unit.

2.2 $C^1\Sigma^+$ state v′, J′ assignment

To assign correctly the $C^1\Sigma$ v', J' levels under study, we first recorded the characteristic fragments of the LIF

$C^1\Sigma^+ - X^1\Sigma^+$ progressions. Note that Ar^+ laser lines induce strong $D^1\Pi - X^1\Sigma^+$ fluorescence as well [7,12,14]. Fortunately, the maximum of the C – X band is shifted to the red spectral region if compared with the main D – X fluorescence region. Simultaneously recorded Ne discharge spectral lines ensured a calibration of the LIF spectra with an absolute wavelength accuracy of about 0.05 nm. Fragments of the recorded spectra were compared to the simulated ones obtained by accounting for the relative intensity distributions within a particular LIF progression. Spectral line positions and Franck-Condon (FC) factors were calculated using accurate empirical $X^1\Sigma^+$ state [7] and $C^1\Sigma^+$ state [13] potentials. The accuracy of experimental line positions and recorded relative intensity distributions were quite sufficient for an unambiguous assignment of the $C^1\Sigma^+$ state v', J' levels. The assignment procedure was greatly facilitated by direct Fourier transform spectroscopy data on the C – X band [13] excited with 514.5 nm line. This line excited transitions to the $v' = 32$–44 range of the $C^1\Sigma^+$ state. It has to be noted that the 501.7 nm laser line excited the $C^1\Sigma^+$ state level with $v' = 46$ [13], but the observed LIF intensity from this level was so weak that it appeared impossible to perform kinetic measurements at reasonable temperatures. The 528.7 nm laser line excited several vibronic $C^1\Sigma^+$ levels giving rather strong C – X fluorescence. We assigned five progressions which started from (v', J') = (24, 19), (25, 46), (25, 51), (26, 69), (32, 40) levels of the $^{23}Na^{85}Rb$ isotopomer.

To reach lower vibrational levels $v' < 10$, a dye laser with Rhodamin 6G dye was used. The laser frequencies required to excite particular v', J' levels were chosen from the list of calculated C – X transitions taking into account the FC factors in the absorbtion. The experimental selection of particular low-lying vibronic levels (see Tab. 1) was complicated by the fact that a strong $B^1\Pi - X^1\Sigma^+$ band, overlapping with the C – X band, could be simultaneously excited in the laser frequency range that was used (17000–17500 cm^{-1}). The dye laser frequency was monitored with a WS6 wavemeter (High Finesse), which provided 0.005 cm^{-1} absolute accuracy. During the experiment the laser frequency was first fixed at a calculated position, or close to it, which caused some molecular fluorescence. After analysis of the recorded spectrum fragment and assignment of the C – X transitions, the laser frequency was slightly adjusted to get the maximal LIF intensity of the selected transition. It turned out that the experimental excitation frequencies determined by our wavemeter readings were typically lower than the calculated ones by ca. 0.02 cm^{-1}, the shift being within Doppler width. Before performing kinetic measurements, the spectral purity around a selected LIF line was re-checked again to confirm detection selectivity.

2.3 Data processing

A typical laser pulse and a LIF decay curve are presented in Figure 2a. A least squares analysis showed that the LIF decay from a selectively excited level was monoexponential as expected. The shaded area in Figure 2a marks the decay region used for processing. The beginning and end of this region are determined by the respective time instants when the laser pulse and LIF intensity drop to the background level. Figure 2b presents an example of the monoexponential fit of LIF decay from the $v' = 2$, $J' = 45$ level of the $^{23}Na^{85}Rb$ $C^1\Sigma^+$ state.

Data processing of LIF decay curves yielded an effective relaxation rate, or the reciprocal effective lifetime τ_{eff}^{-1} of a rovibronic level at a particular temperature. One may neglect the effect of flight-out-of-view of excited molecules [17] since the ratio of the mean velocity of the molecules $\overline{v}_0$ to laser beam width d_0, the laser beam width being about 1 mm, is $\overline{v}_0/d_0 \sim 2 \times 10^4 s^{-1}$, is about three

Table 1. Radiative lifetimes τ_{rad} for the $^{23}Na^{85}Rb$ $C^1\Sigma^+$ levels excited in $C^1\Sigma^+(v', J') - X^1\Sigma^+(v'', J'')$ transitions induced by $\widetilde{\nu}_{exc}/\lambda_{exc}$ laser line.

$\widetilde{\nu}_{exc}/\lambda_{exc}$	v'	J'	v''	J''	$\tau_{rad} \pm \Delta\tau_{rad}$, ns
17096.91 cm^{-1}	2	45	5	46	61.0 ± 2.7
17222.50 cm^{-1}	4	51	5	50	55.2 ± 1.5
17539.94 cm^{-1}	8	64	4	63	52.0 ± 1.2
528.7 nm	24	19	1	18	51.1 ± 1.8
	25	46/51*	1	47/50	54.5 ± 1.9
	26	69	1	68	44.7 ± 2.3
514.5 nm	32	43	0	42	43.6 ± 1.0
	33	8	1	9	43.1 ± 1.5
	34	42	1	43	40.7 ± 1.5
	35	10	2	11	41.1 ± 0.7
	35	63	1	62	42.2 ± 1.4
	39	26	4	25	39.8 ± 0.9
	41	23	5	24	37.2 ± 0.8
	44	96	4	95	33.9 ± 0.8

* measured on two overlapping lines with $J' = 46$, 51.

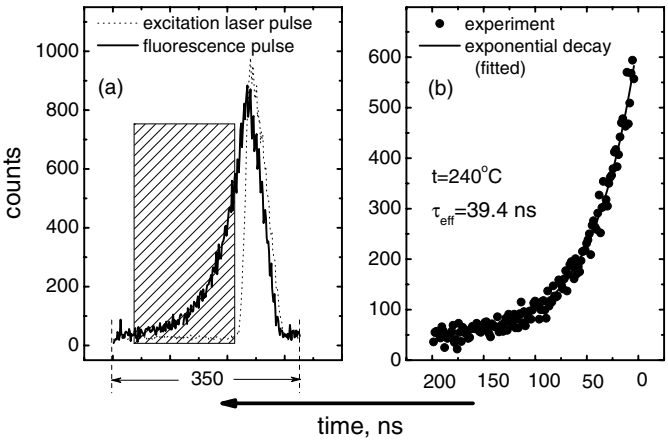

Fig. 2. Typical laser pulse and fluorescence decay kinetic signals recorded at inverse start-stop regime, see text. (a) Excitation pulse and LIF response and (b) LIF decay monoexponential fitting for the $^{23}Na^{85}Rb$ $C^1\Sigma^+$ ($v' = 2$, $J' = 45$) level.

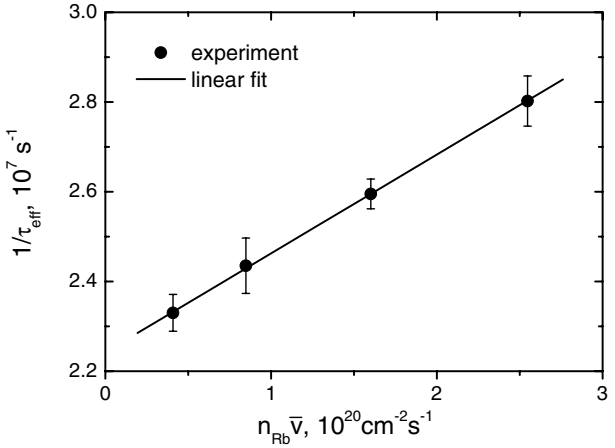

Fig. 3. Stern-Volmer plot of the inverse effective lifetime τ_{eff}^{-1} for the ^{23}Na^{85}Rb $C^1\Sigma^+$ ($v' = 26$, $J' = 69$) level as dependent on Rb atom concentration $n_{\rm Rb}$ times mean relative velocity $\overline{v}$ (see Eq. (1)). Fitting parameters: $\sigma = 2.2 \times 10^{-14}$ cm^2, $\tau_{rad} = 44.7$ ns.

orders of magnitude smaller than τ_{eff}^{-1}. Collisionless radiative lifetime values τ_{rad} were obtained by varying the temperature within the 180–280 °C range and extrapolating to zero the concentration of Rb atoms $n_{\rm Rb}$, see Figure 3, according to

$$\frac{1}{\tau_{eff}} = \frac{1}{\tau_{rad}} + n_{\rm Rb}\sigma\bar{v}, \qquad (1)$$

σ being the effective quenching cross-section, $\bar{v} = \sqrt{8kT/\pi\mu}$, the mean relative velocity of the colliding partners assuming Maxwellian velocity distribution, μ, the reduced mass, and k, the Boltzman constant. The population quenching of the $C^1\Sigma^+$ v', J' rovibronic level by Rb atoms was considered as a prevailing collision process since Rb concentration was about two orders of magnitude higher than the concentration of Na, Na_2, and Rb_2 [18]. The possible systematic inaccuracy in measuring the concentration is estimated as ca. 10%. The τ_{eff}^{-1} dependencies on $n_{\rm Rb}$ have been obtained for eleven v', J' levels within the v' range from 24 to 44. Several measurement series performed in two different cells showed rather a large dispersion of σ values and did not allow us to reveal any σ dependence on v'. Hence we report here for the $C^1\Sigma^+$ state an effective collisional cross-section value $\sigma = (3 \pm 1) \times 10^{-14}$ cm^2 averaged over all involved v', J' levels. This σ value was used to obtain radiative lifetime values for three lower $v' = 2$, 4, and 8 levels, for which the τ_{eff} measurements were performed at 240 °C temperature. The measured τ_{rad} values for a total of 14 levels of the ^{23}Na^{85}Rb isotopomer are given in Table 1. Reported uncertainties represent statistical errors within the 95% confidence interval estimated from several measurement series, as well as a contribution from the uncertainty in σ.

3 Calculation

The radiative lifetime τ_{rad} for a particular rovibronic level v', J' of the $C^1\Sigma^+$ state is defined [19] as the sum over the emission Einstein coefficients $A_{iv'J'}^{jv''J''}$ for all bound and embedding continuum lower-lying j, v'', J'' rovibronic states:

$$\frac{1}{\tau_{rad}^i} = \sum_j \sum_{v''} \sum_{J''} A_{iv'J'}^{jv''J''}, \qquad (2)$$

$$A_{iv'J'}^{jv''J''} = \frac{8\pi^2}{3\hbar\epsilon_0} \left(\nu_{iv'J'}^{jv''J''}\right)^3 |\langle v_i'(J')|d_{ij}|v_j''(J'')\rangle|^2 \frac{S_{J'J''}}{2J'+1},$$

where $i \in C^1\Sigma^+$ and $j \in [B^1\Pi$, $c^3\Sigma^+$, $A^1\Sigma^+$, $b^3\Pi$, $a^3\Sigma^+$, $X^1\Sigma^+]$, $\nu_{iv'J'}^{jv''J''} = E_i^{v'J'} - E_j^{v''J''}$ is the transition wavenumber, $S_{J'J''}$ is Hönl-London factor available in an analytical form, $d_{ij}(R)$ is the transition dipole moment, and $E^{v,J}$ and $|v(J)\rangle$ are the rovibronic energies and rovibrational wave functions of the upper i and lower j electronic states.

It appears that the contribution of the $C^1\Sigma^+$ – $B^1\Pi$ transition into the total lifetime of the $C^1\Sigma^+$ state can be neglected since the $B^1\Pi$ state has a minimal energy gap as compared to other excited states (see Fig. 1). The singlet-triplet $C^1\Sigma^+$ – c, $a^3\Sigma^+$ transitions are strictly forbidden in a pure Hund's (**a**) coupling case [19]. Although the $C^1\Sigma^+$ – $b^3\Pi$ transition is also forbidden, an influence of the $b^3\Pi$ state on the C – A transition probabilities and lifetimes τ_{rad} seems to be worth analysing because of the full mixing of the $A^1\Sigma^+$ and $b^3\Pi$ states caused by the strong spin-orbit coupling effect [11,20].

The required singlet-singlet $C^1\Sigma^+$ – X,$A^1\Sigma^+$ transition dipole moment functions were computed in the framework of the second order many-body multipartitioning perturbation theory [21] with an explicit treatment of the core-valence correlation effects. The present computational scheme based on the Hund's (**a**) case representation of the electronic states was exactly the same as the one used in our previous study of NaRb [6] also the Gaussian basis set $(7s7p5d3f)$Na, Rb, used here was chosen from [11]. This basis set was slightly more flexible and better suited for reproducing electronic energy and transition moments. The resulting MPPT pointwise $d_{C-X,A}(R)$ functions were calculated in the interval $R \in [3.0, 7.0]$ Å, see Table 2 and Figure 4. The CPP $d_{C-X}(R)$ moment calculated in a wide R-interval [22] is presented in Figure 4. The sudden drop of this function between 8 Å and 10 Å reflects avoided crossing of the adiabatic $C^1\Sigma^+$ and $E^1\Sigma^+$ states having strong ionic/covalent mixing character. This function was also applied to estimate the A_C^X transition probabilities in order to test the consistency of both the MPPT and CPP estimates.

The eigenvalues and eigenfunctions of the isolated $C^1\Sigma^+$ and $X^1\Sigma^+$ states were calculated in the framework of standard adiabatic approximation [19] using highly accurate empirical PECs available for the ground [7] and $C^1\Sigma^+$ [13] states, respectively. The nonadiabatic energies $E_{A\sim b}^{vJ}$ and wavefunctions $f_k^J(R)$ ($k \in [A^1\Sigma^+, b^3\Pi_0, b^3\Pi_1, b^3\Pi_2]$) belonging to the different components of the fully

Table 2. The MPPT $C^1\Sigma^+ - X^1\Sigma^+$ and $C^1\Sigma^+ - A^1\Sigma^+$ transition dipole moments (in a.u.).

R(Å)	C – A	C – X
3.01631	2.786	0.860
3.12215	2.830	0.867
3.25973	2.849	0.882
3.38673	2.830	0.906
3.51374	2.778	0.934
3.64338	2.692	0.970
3.78891	2.557	1.017
3.90533	2.424	1.058
4.02175	2.272	1.105
4.17669	2.041	1.173
4.31809	1.816	1.242
4.44509	1.599	1.306
4.70968	1.138	1.446
4.97427	0.695	1.589
5.23885	0.298	1.723
5.76803	–0.357	1.941
6.08554	–0.712	2.045
6.40304	–1.134	2.145
6.69409	–1.701	2.249
7.01160	–2.790	2.378

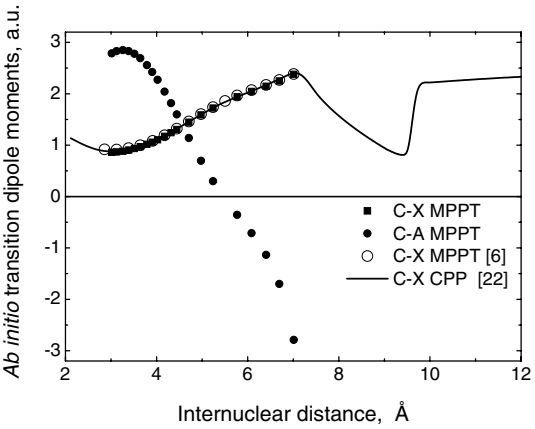

Fig. 4. Ab initio $C^1\Sigma^+ - X^1\Sigma^+$ and $C^1\Sigma^+ - A^1\Sigma^+$ transition dipole moment functions *d(R)* for NaRb molecule.

mixed $A^1\Sigma^+ \sim b^3\Pi$ complex were obtained by a close-coupling calculation. It was based on the adiabatic $U_A(R)$, $U_b(R)$ PECs and spin-orbit coupling matrix elements derived in reference [11] by a direct deperturbation analysis of the experimental A ∼ b term values. The Einstein coefficients for a C – A ∼ b transition were evaluated as

$$A^{A\sim bv''J''}_{Cv'J'} = \frac{8\pi^2}{3\hbar\epsilon_0}\left(E^{v'J'}_C - E^{v''J''}_{A\sim b}\right)^3 \times |\langle v_C(J')|d_{C-A}|f_A(J'')\rangle|^2 \frac{S_{J'J''}}{2J'+1}, \quad (3)$$

where $f_A(J)$ is the fraction of the $A^1\Sigma^+$ state in the total non-adiabatic wave function.

It should be noted that the straightforward summation of equation (2) could not be done easily for the high

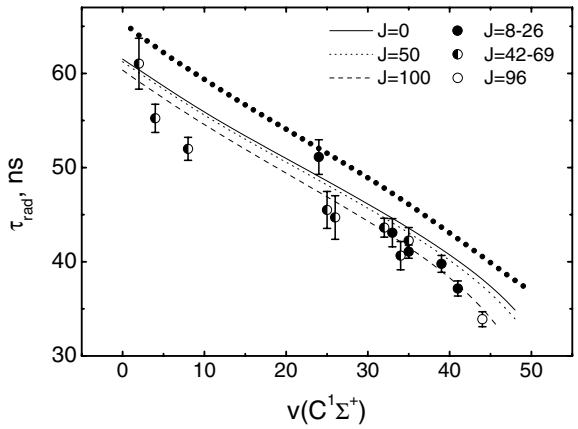

Fig. 5. Comparison of experimental radiative lifetime values (circles) of the NaRb $C^1\Sigma^+$ v', J' levels with ab initio calculated $\tau_{rad}(v')$ dependencies (lines). The upper dotted curve is obtained (for $J = 0$) when the C – A transitions are ignored in the calculations.

vibrational v_C levels since the required sum of the corresponding FCF values $\sum_{v''} |\langle v_C|v''\rangle|^2 = 1$ converges very slowly. In particular, 78 vibrational levels of the ground state and about 160 levels of the $A \sim b$ complex are needed to satisfy the sum $\sum_{v''} |\langle v_C|v''\rangle|^2 \geq 0.998$ for the $v_C \geq 40$ levels. In practice, this requirement means that the solution of equation (2) requires a knowledge of all relevant PECs and transition moments over a very wide range of internuclear distances. This drawback, which is related to an almost complete eigenstate problem for lower electronic states, has been overcome by the approximate sum rule [23,24]:

$$\frac{1}{\tau^C_{rad}} \approx \frac{8\pi^2}{3\hbar\epsilon_0}\langle v_C(J')|\left[\sum_{j\in X,A} \Delta U^3_{C-j} d^2_{C-j}\right]|v_C(J')\rangle, \quad (4)$$

where the $\Delta U_{ij}(R) = U_i(R) - U_j(R)$ is the difference between the corresponding adiabatic PECs. The radiative lifetimes τ_{rad} calculated by equation (4) as the expectation value of the $\sum_{j\in X,A} \Delta U^3_{C-j} d^2_{C-j}$ operator defined in the interval $R \in [3, 7]$ Å are presented in Figure 5 for the $0 \leq v_C \leq 45$ levels.

The numerical tests specially performed for the lowest $0 \leq v_C \leq 30$ levels ($\sum_{v''} |\langle v_C|v''\rangle|^2 > 0.9999$) have indicated that equation (4) is correct within 0.1% for both adiabatic C – X and non-adiabatic C – A ∼ b transitions. The reliability of the adiabatic approximation for the A^A_C estimates follows from the fact that the non-adiabatic wave functions of the $A^1\Sigma^+$ state can be approximated as $f_A(J) \approx C_k|v_A(J)\rangle$, where $|v_A(J)\rangle$ is the adiabatic wave function and the C_k are the R-independent mixing coefficients, which obey the normalization condition $\sum_k^4 C_k^2 = 1$ for each component of the complex. Then, the sum of the non-adiabatic Einstein coefficients over all components of the A ∼ b complex at fixed J'' value could be approximated as $\sum_k^4 (E_C - E_k)^3 C_k^2 |\langle v_C|d_{C-A}|v_A\rangle|^2 \approx (E_C - E_A)^3 |\langle v_C|d_{C-A}|v_A\rangle|^2$, where a difference between

the adiabatic E_A and non-adiabatic E_k energy of the $A^1\Sigma^+$ state is neglected.

4 Discussion

Figure 5 demonstrates rather good agreement between experimental and theoretical lifetimes for most rovibronic $C^1\Sigma^+$ state levels. Both experimental and calculated $\tau_{rad}(v', J')$ values monotonically decrease from about 61 to 34 ns as the vibrational quantum number increases from $v' = 2$ to 44. The theory predicts a weak systematic decrease of τ_{rad} values by ca. 1.5–3 ns as the J' value increases from $J' = 0$ to 100. The small systematic overestimation of the calculated τ_{rad} values could be attributed to an uncertainty of the ab initio transition moments (ca. 1–3%, see Fig. 4) and to a systematic uncertainty of about 1% in the experimental time scale calibration of the measuring system. The $1/A_C^X$ values calculated using the present and preceding [6] MPPT transition moments as well as the CPP transition moment $d_{C-X}(R)$ [22] did not differ by more than 0.5–1.0 ns.

The present calculations prove that the main contribution (>90%) to the lifetime values of the $C^1\Sigma^+$ state comes from the $C^1\Sigma^+ - X^1\Sigma^+$ transition, while the $C^1\Sigma^+ - A^1\Sigma^+ \sim b^3\Pi$ transition diminishes the lifetimes by only 2.0–3.5 ns, see Figure 5. The strong spin-orbit coupling of the $A^1\Sigma^+$ and $b^3\Pi$ states does not affect the lifetimes of the $C^1\Sigma^+$ state, although it leads to the pronounced relative intensity redistribution in the rovibronic transitions between the C state and the different components of the $A \sim b$ complex.

It should be noted that the present study of radiative properties of the NaRb $C^1\Sigma^+$ state is limited to the vibrational levels localized in the interval $R \in [3, 7]$ Å and, hence, the abrupt change of the C – X transition dipole moment beginning at $R > 7.5$ Å (Fig. 4) does not affect the lifetimes of the $v'_C \leq 44$ levels involved in this work. The pronounced increase of the τ_{rad} values should be expected for the $v'_C \geq 45$ levels in the shelf region (see Fig. 1), while the lifetimes of the higher v' levels near the Na($3p$)+Rb($5s$) dissociation threshold should again decrease towards 16.4 ns, which is the lifetime of the Na($3p$) atom [25]. It is worth mentioning that the $C^1\Sigma^+$ NaRb radiative lifetimes are considerably larger, within a comparable v' range, than the τ_{rad} values of ca. 22–17 ns for the $D^1\Pi$ states of NaRb [14] and NaK [26] molecules converging to the dissociation limit involving the Na($3p$) atom. The present effective collisional quenching cross-section value is close to the $(3 - 6) \times 10^{-14}$ cm^2 value obtained in [14] for NaRb($D^1\Pi$) + Rb collisions.

The authors are indebted to Dr. O. Dulieu for providing the unpublished CPP C – X transition dipole moment function, as well as to Prof. M. Auzinsh and Dr. F. Gahbauer for numerous useful discussions, and to O. Martinsons and E. Gevelis for assistance during the experiments. This work has been supported by the NATO SfP-978029 *Optical Field Mapping* grant. The Riga team acknowledges funding from the EC 5th Frame Growth Grant G1MA-CT-2002-04063 and from the Latvian Council of Science (grant No. 04.1308).

References

1. H. Wang, W.C. Stwalley, J. Chem. Phys. **108**, 5767 (1998)
2. S.B. Weiss, Bhattacharya, N.P. Bigelow, Phys. Rev. A **68**, 042708 (2003)
3. W.C. Stwalley, Eur. Phys. J. D **31**, 221 (2004)
4. S. Azzizi, M. Aymar, O. Dulieu, Eur. Phys. J. D **31** 195 (2004)
5. M. Korek, A.R. Allouche, M. Kobeissi, A. Chaalan, M. Dagher, K. Fakherddin, M. Aubert-Frecon, Chem. Phys. **256**, 1 (2000)
6. A. Zaitsevskii, S.O. Adamson, E.A. Pazyuk, A.V. Stolyarov, O. Nikolayeva, O. Docenko, I. Klincare, M. Auzinsh, M. Tamanis, R. Ferber, R. Cimiraglia, Phys. Rev. A **63**, 052504 (2001)
7. O. Docenko, M. Tamanis, R. Ferber, A. Pashov, H. Knöckel, E. Tiemann, Phys. Rev. A **69**, 042503 (2004)
8. A. Pashov, O. Docenko, M. Tamanis, R. Ferber, H. Knöckel, E. Tiemann, Phys. Rev. A **72**, 062505 (2005)
9. Y.-C. Wang, M. Kajitani, S. Kasahara, M. Baba, K. Ishikava, H. Katô, J. Chem. Phys. **95**, 6229 (1991)
10. Y.-C. Wang, K. Matsubara, H. Katô, J. Chem. Phys. **97**, 811 (1992)
11. M. Tamanis, R. Ferber, A. Zaitsevskii, E.A. Pazyuk, A.V. Stolyarov, H. Chen, J. Qi, H. Wang, W.C. Stwalley, J. Chem. Phys. **117**, 7980 (2002)
12. O. Docenko, M. Tamanis, R. Ferber, A. Pashov, H. Knöckel, E. Tiemann, Eur. Phys. J. D **36**, 49 (2005)
13. W. Jastrzebski, P. Kortyka, P. Kowalczyk, O. Docenko, M. Tamanis, R. Ferber, A. Pashov, H. Knöckel, E. Tiemann, Eur. Phys. J. D **36**, 57 (2005)
14. I. Klincare, M. Tamanis, R. Ferber, Chem. Phys. Lett. **382**, 593 (2003)
15. M. Jansons, J. Klavins, Zh. Kharcheva, M. Tamanis, Phys. Scr. **45**, 328 (1992)
16. S. Kasahara, T. Ebi, M. Tanimura, H. Ikoma, K. Matsubara, M. Baba, H. Katô, J. Chem. Phys. **105**, 1341 (1996)
17. M.P. Auzinsh, M.Ya. Tamanis, R.S. Ferber, Ya.A. Kharya, Opt. Spectrosc. (USSR) **67**, 750 (1989)
18. A.N. Nesmeyanov, *Vapour Pressure of Chemical Elements*, (Izd. Akad. Nauk SSSR, Moscow, 1961) (in *Russian*)
19. H. Lefebvre-Brion, R.W. Field, *The Spectra and Dynamics of Diatomic Molecules* (Academic Press, New York, 2004)
20. A. Jarmola, M. Tamanis, R. Ferber, E.A. Pazyuk, A.V.S tolyarov, J. Q. S. R. T. **95**, 165 (2005)
21. A. Zaitsevskii, R. Cimiraglia, Int. J. Quant. Chem. **73**, 395 (1999)
22. O. Dulieu, private communication
23. J. Tellinghuisen, P.S. Julienne, J. Chem. Phys. **81**, 5779 (1984)
24. A.V. Stolyarov, V.I. Pupyshev, Phys. Rev. A **49**, 1693 (1994)
25. C.E. Theodosiou, Phys. Rev. A. **30**, 2881 (1984)
26. M. Tamanis, M. Auzinsh, I. Klincare, O. Nikolayeva, R. Ferber, A. Zaitsevskii, E.A. Pazyuk, A.V. Stolyarov, J. Chem. Phys. **109**, 6725 (1998)